Tectonophysics 860 (2023) 229906

Contents lists available at ScienceDirect

Tectonophysics

journal homepage: www.elsevier.com/locate/tecto

3-D density structure of the upper-mantle in the eastern Mediterranean Sea and surrounding region using gravity inversion constrained by seismic velocity model

Fayez Harash [a,b,*], Chao Chen [a,c], Liang Qing [a,c], Chenming Tu [a], Al-Ansari Nadhir [d,*], Amin Khalaf [e], Imad ALrawi [f], Aref ALshameri [g]

[a] State Key Laboratory of Geological Processes and Mineral Resources, School of Geophysics & Geomatics, China University of Geosciences, Wuhan 430074, China
[b] Geology Department, Faculty of Sciences, Damascus University, Damascus 0100, Syria
[c] Hubei Subsurface Multi-Scale Imaging Key Laboratory, School of Geophysics & Geomatics, China University of Geosciences, Wuhan 430074, China
[d] Water Resources Engineering, Department of Civil, Environmental and Natural Resources Engineering, Lulea University of Technology, Lulea 971 87, Sweden
[e] Sorbonne Universite, EPHE, Milieux Environnementaux, Transferts et Interactions dans les hydrosyst´emes et les Sols, METIS F-75005, France
[f] School of Earth Sciences and Resources, China University of Geosciences (Beijing), Beijing 100083, PR China
[g] Faculty of Petroleum and Natural Resources, Sanaa University, Sanaa, Yemen

ARTICLE INFO

Keywords:
Density Structure
Eastern Mediterranean Sea
Gravity Inversion
Lithospheric
Upper Mantle

ABSTRACT

A 3D density structure of the lithosphere and upper mantle beneath the eastern Mediterranean Sea (EMS) and its adjacent region was constructed based on gravity anomaly inversion constrained by a seismic tomography model. Gravity effects of terrain and crust were removed from the observed gravity field (EIGEN-6C4) to obtain the residual mantle gravity anomaly (RMGA). The density distribution of the lithosphere and upper mantle was investigated. The 3D inversion process was constrained by an initial density model projected from the shear-wave velocity model (SL2013sv). The results show some characteristics of the density distribution in the lithosphere and in the upper mantle that could be related to the tectonic importance of the Mediterranean Sea and the surrounding region. A low-density zone dominates the lithosphere beneath the Sea except for the area around the Arabia Shield and North Anatolian Fault belt. A thinner, high-density layer beneath the southwest of the Sea may be related to the older oceanic lithospheric fragments. The high-density anomalies appear at depths below 280 km beneath the Sea and the Turkish Aegean Sea Plate. However, the low-density anomalies appear on the upper mantle under the trenches of the southwestern part of the Mediterranean Sea, the eastern part of the Aegean Sea, the Red Sea, the Black Sea, and the middle of the Arabia shield. The deep structure under the Eratosthenes seamount in the Mediterranean Sea is the source of the intensity and genesis of tectonic activity. Furthermore, the convergence region of two low-density anomaly zones (Africa-Anatolia) may be interpreted as a significant tectonic unit (Eratosthenes seamount) caused by the arrival of the relatively thick and buoyant Eratosthenes block to its present location south of Cyprus in Holocene time based on the density model interpretation beneath the Mediterranean Sea during the Late Cretaceous and early Tertiary period.

1. Introduction

The tectonic setting of the Middle East is still active represented by its tectonic boundaries. These boundaries in the east comprise thrust belt and the Zagros fold that forms the collision zone between the Arabian plate and Iran, in the west there are active subduction zones along the Hellenic and Cyprus trenches, in the north the East Anatolian Fault, in the south of the Red sea and the Dead Sea continental transform fault that separate the Arabian plate from the Levantine microplate (Brew et al., 2003). Folding in the sediments, faulting in the basement and strike-slip movements in the Anatolian and Iranian Plateaus are the main responsible factor affecting the convergence between Arabian and Eurasian plates and structural evolution of the upper-mantle beneath the Mediterranean Sea and the surrounding regions. There are many clear

* Corresponding author at: State Key Laboratory of Geological Processes and Mineral Resources, School of Geophysics & Geomatics, China University of Geosciences, Wuhan 430074, China.
E-mail addresses: f.harash@cug.edu.cn (F. Harash), nadhir.alansari@ltu.se (A.-A. Nadhir).

https://doi.org/10.1016/j.tecto.2023.229906
Received 8 February 2023; Received in revised form 18 April 2023; Accepted 5 May 2023
Available online 15 May 2023

features in the region because of this complicated history as Dead Sea which separates the Arabian and the African plates. The tectonic movement of the plates boundaries controls the tectonic deformation in the region especially in Syria that is observed in the Palmyride fold and the Euphrates system (Barazangi et al., 1993), the plate. This movement could be described as vertical perturbation leading to cause the extensional deformation in the Mediterranean Sea (Flerit et al., 2004; Barbot and Weiss, 2021).

The movement rate around 18 mm/y for the African plate in the northeast direction and about 6 mm/yr for the Arabian plate (Di Luccio and Pasyanos, 2007). Levant basin was opened in the EMS as a result of the separation of the Arabian plate from the African plate. The existence of an expansive diversity of plate boundaries and tectonic settings give us the chance to look for the dynamic interactions between tectonic frameworks so we need a complete information and data about the lithosphere structure and the upper mantle of the study area.

The Eastern Mediterranean (EMS) is one of the complex regions that has experienced to tectonic deformation according to its location between the African, Arabian, and Eurasian tectonic plates, where the African lithosphere is subducted along the Mediterranean Ridge and expands along the Dead Sea Fault System (DSFS) in the northwestern Arabian plate (Barbot and Weiss, 2021). The northwestern part of the Arabian plate is a very interesting region as well, because of its tectonic separation from the African plate in the south and the collision with the Anatolian microplate in the north, including the Red Sea spreading and its movement in the Suez Gulf (Fig. 1) and the Dead Sea rift (Ben-Avraham, 1985).

The eastern Mediterranean region has a complicated geological history that extended from late Triassic to early Jurassic ages (Garfunkel, 1998). The various stratigraphic evolution of the eastern Mediterranean region represents the complicated Cenozoic and pre-Cenozoic boundaries (McBRIDE, 1990). The Dead Sea Fault System (DSFS) starts in the south from northern part of Aqaba Gulf to Kara Su Valley in the north with a total length about 1100 km crossing four countries, through the Arab Wadi, Jordan Valley in Jordan, the Beqa'a Valley in Lebanon and AL-Ghab Graben in Syria. That is considered as north-south, left-lateral strike shear zone as it binds the northwestern part of the Arabian plate (Smit et al., 2010; Agrawal et al., 2015) (Fig. 1). Density heterogeneities are firmly related with tectonic procedures especially in the upper-mantle, as density varieties cause huge stresses that play a big role in the crustal movements and lithosphere deformations (Kaban et al., 2015). Density might be different because of the stress caused by movement discrepancy between upper-mantle and trench. Compositional, structural, and thermal anomalies are generated because of incessant interactions of mantle and plate. To know more about tectonic processes and their surface appearance we need more understanding of mantle density contrast because seismic tomography model is more sensitive to temperature than composition.

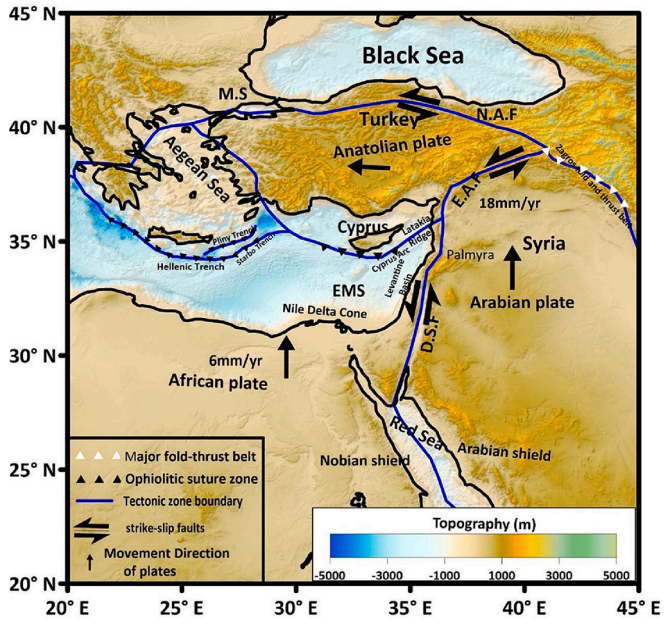

Fig. 1. Location of the study area (WMS Demo Server), Simplified tectonic and topographic map of the Eastern Mediterranean. Thick lines show the main plate boundaries. Approximate plate velocity vectors are shown in red (Stern and Johnson, 2010). N.A.F = North Anatolian Fault; E.A.F = East Anatolian Fault; D. S. F = Dead Sea Fault; MS = Marmara Sea; EMS = Eastern Mediterranean Sea. (For interpretation of the references to colour in this figure legend, the reader is referred to the web version of this article.)

The Eratosthenes Seamount (ESM) is considered as carbonate platform appeared on the continental African Plate fragment that separated from the Pangaea supercontinent since the Triassic (Makris et al., 2021; Klimke and Ehrhardt, 2014; Galindo-Zaldívar et al., 2001; Garfunkel, 1998) and it has been entranced close to Cyprus in the duration of Pliocene–Pleistocene. Therefore, those two reasons were responsible to result a new regime in the plate tectonic from subduction to continent –continent collision and Cyprus uplift later during the same geological period itself (Klimke and Ehrhardt, 2014; Schattner, 2010; Robertson Alastair, 1998).

There are previous various regional gravity and tomography studies which have studied upper mantle beneath many regions in the middle east (Berk Biryol et al., 2011; Simmons et al., 2015; Tang et al., 2019; Seber et al., 2001) but their results have shortcoming because of their limited study areas and lack of data in the Middle East. Gravity models had a lot of problems due to irregular terrestrial observations and changeable data (Kaban and Yuanda, 2014). The current geophysical researches in the Middle East are constantly developing. Fortunately, gravity models of the upper mantle in the Middle East have got one benefit that almost all offered seismic data integrated into 3D crustal model.

The location of subduction zones and trenches can be figured out by the high seismic velocity, but still we need density variations to determine thermal and composition structure of the upper- mantle (Root et al., 2017). Gravity data collected from GRACE and GOCE satellite missions is an important tool that helps us to invert the density variations to study the interior of the earth. Recently, many results have been obtained depending on using seismic velocity and gravity data to determine the structure of the lithosphere and asthenosphere (Mooney and Kaban, 2010; Chaves and Ussami, 2013; Kaban et al., 2016a, 2016b; Liang et al., 2019).

In this study, we first calculate mantle gravity anomaly which can reflect the upper-mantle density variation after removing the effects of terrain, crust and deep mantle (Kaban et al., 2016a, 2016b) from the free-air gravity anomaly (FAG) (Fig. 2). Then a 3-D density model of the upper-mantle in the EMS and the adjacent regions is constructed, by using the 3-D gravity inversion algorithm (Liang et al., 2019) to investigate the upper-mantle density distribution beneath the EMS and surrounding regions and reveal the probable geological implications. The calculated anomaly gives us an overview about the contrasts of the upper mantle density. The initial density model is built depending on seismic tomography model of Schaeffer and Lebedev (2013), because seismic tomography model is more sensitive to temperature than composition. A significant target of our investigation is to give such a cohesive density map for the study area.

2. Method

2.1. Mantle gravity anomaly

The upper mantle gravity anomaly previously corrected and computed by Kaban et al. (2016a, 2016b) was used in this study to eliminate the gravitational effects of the crust and deep mantle from the

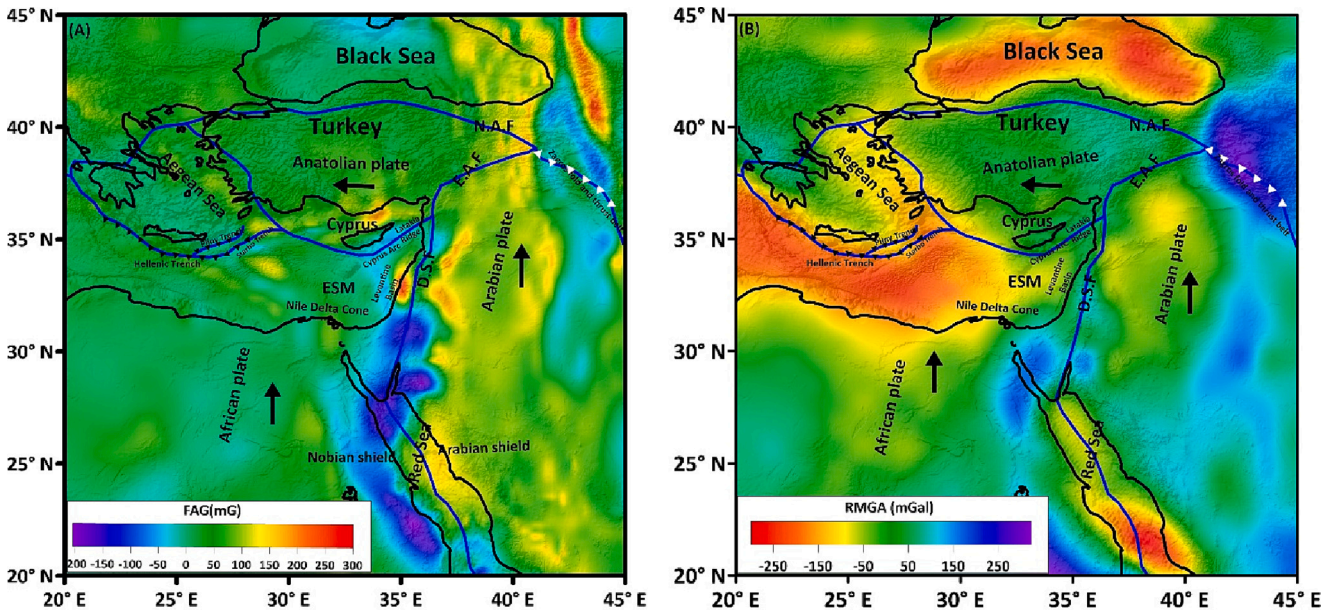

Fig. 2. (A) Free air gravity (FAG) and (B) (RMGA) Residual mantle gravity anomaly (Kaban et al. 2016) after removing the effects of topography/bathymetry, sediments, crustal density variation and the Moho relief from the free air gravity anomaly (EIGEN-6c4 model, Forste et al., 2014).

EIGEN-6c4 gravity field model (Förste et al., 2014). Fig. 2A shows the distribution of FAG over the EMS and surrounding regions. Higher values were noticed over Tiberias Lake and Cyprus (over 150 mGal), while lower values of free air gravity were found over the northern part of the Red Sea and southeast of Cyprus Island (−100 mGal). This represents deep-sea locations. Density contrast was regarded as an essential metric that played a considerable effect in the impact of gravity anomalies. It is possible to differentiate the lithology by analyzing its conduct while varying the depth. The gravity anomalies attributed to terrain, sediments, crystalline crust, Moho relief, and deep mantle have been calculated and removed from FAG to reflect the heterogeneous density variation in the upper mantle. According to the 1D continental reference model shown in Table 1 (Kaban et al., 2016a, 2016b), the crust contains two crustal layers (0–15 km with 2.7 g cm^{-3} and 15–40 km with 2.94 g cm^{-3}) constrained to the upper mantle with a density of 3.357 g cm^{-3}. This continental reference model is equalized in the isostatic case with oceanic crust–upper mantle tectonic that goes back to 180 Ma based on the conserving-plate model (Kaban and Schwintzer, 2001). Therefore, when we use these oceanic and continental models, the gravity effect of layers from crust to Moho discontinuity depth will be the same. The crustal model (Stolk et al., 2013) computes the crustal gravity effects, while the whole mantle seismic tomography model S40RTS (Ritsema et al., 2011) has been used in Kaban et al. (2014a) to calculate the gravity effects of the deep mantle. After removing these effects from the observed field, the residual mantle gravity anomalies (RMGA) were calculated.

Fig. 2B shows the RMGA calculated after correcting terrain, crust, and deep mantle. Minimum solid anomalies were observed in the Red Sea and the Gulf of Aden. A gravity minimum is associated with a triple junction resulting from severe mantle upwelling. The minimum anomaly extends in the western EMS associated with plate Collison zones like the Cyprian trenches, the Pliny, and the Strabo trenches. The maximum values of RMGA were located in the northern part of the Red sea and at the northeastern part of the Arabian plate.

2.2. The thermal model

The mineral physics approach of Stixrude and Lithgow-Bertelloni (2005), (Kaban et al., 2014) as weight average of the Mg, Fe, and Ca, has been used to convert velocity seismic *Vs* variations SL2013sv seismic tomography into temperatures and related density variations (Schaeffer and Lebedev, 2013). According to previous studies (Lee, 2003; Kaban et al., 2014; Tesauro et al., 2014), compositional differences can produce both positive and negative density anomalies in the upper mantle, depending on the local thermal regime. The residual topography (t_{res}), which is considered to be the part of the topography or bathymetry that is not balanced by the crustal structure and includes changes of the crust-mantle boundary, is also estimated using the density model of the crust (Kaban et al., 2004):

$$t_{res} = \frac{1}{\bar{\rho}}(\rho_{top})t_{obs} + \frac{1}{\bar{\rho}}\int_0^M \Delta\rho(h)\left(\frac{R-h}{R}\right)^2 dh \quad (1)$$

Where ρ_{top} denotes the average block density above sea level (with the effect of sediments and ice); t_{obs} defines as the topography (zero offshore); R represents the Earth radius; $\rho = 2670$ kg/m^3 is the average density; $\Delta\rho(h) = \rho - \rho_{ref}$ is the density anomaly relative to a horizontally reference model; and h is the depth from sea level.

The residual topography is generally related with the density structure of the mantle lithosphere and with dynamic topography supported by the mantle convection (Steinberger and Calderwood, 2006).

The computed t_{res} is used to constrain 3D density model of the upper-mantle by employing the mantle gravity anomalies and residual topography. Occam's inversion is reformulated to derive the initial density from seismic tomography (Kaban et al., 2013; Kaban et al., 2014).

$$min\{\|A\rho - g_{res}\|^2 + k\|B\rho - t_{res}\|^2 + \alpha\|\rho - \rho_{ini}\|^2\} \quad (2)$$

Table 1
1-D reference density model of the crustal and upper mantle effects.

Depth (km)	0–15	15–40	50	100	150	200	250	300
Density (g.cm^{-3})	2.7	2.94	3.357	3.384	3.419	3.457	3.510	3.560

where A is the integral operator that transforms variations in density into gravitational anomalies (Kaban, 2011), B is the integral operator that converts density variations to topography undulations, t_{res} is the residual topography. g_{res} is the residual gravity field. $k = 2\pi G\rho_t$ is the scaling factor normalizing for topographic variation in relation to gravity (G is the gravitational constant) and α is defined as the damping factor.

In order to convert seismic velocity into temperature, the anharmonic velocity was estimated including four major mineral phases as (Ol,OPX,CPX and Gt) (Kaban et al., 2014). Every one was considered as an ideal solid solution of Mg, Fe, Gt and Ca where Ol(forsterite and fayalite), CPX(diopside and Hedenbergite), OPX(enstatite) and Gt(Pyrope, almandine and glossularz. The pahses perecentage differ with variation of Mg. The STP condition has twofold which are the pressure take of each phase at zero pressure (P_0) and $T_0 = 300$ k at room temperature (Cammarano et al., 2003). all parametes are subjected to STP conditions (Stixrude and Lithgow-Bertelloni, 2005):

$$P_{TOT}(V,T) = P_{ref}(V) + \Delta P_{th}(V,T) \tag{3}$$

$P_{TOT}(V,T)$ is defined as the total pressure, P_{ref} is the pressure at reference temperature (isotherm at 300 k) and ΔP_{th} is the thermal pressure. Isothermal compression is obtained by the third-order Birch-Murnaghan formula (Stixrude and Lithgow-Bertelloni, 2005):

$$P_{st} = \frac{3}{2}K_{T_0}\left[\left(\frac{V_0}{V}\right)^{7/3} - \left(\frac{V_0}{V}\right)^{5/3}\right]\left\{1 - \frac{3}{4}\left(4 - K'_{T_0}\right)\left[\left(\frac{V_0}{V}\right)^{2/3} - 1\right]\right\} \tag{4}$$

V is expressed as the molar volum at temperature T. By applying the Debye model (Jackson and Rigden, 1996) we obtain the thermal pressure as follow:

$$\Delta P_{th} = \frac{\gamma(V)}{V}\left[E_{th}(V,T) - E_{th}(V,T_0)\right] \tag{5}$$

γ is defined as Gruneisen parameter,which specifies how altering a crystal's volume affects its vibrational properties and, consequently, how altering temperature affects the size or dynamics of the lattice. It is simplified as:

$$\gamma = \gamma_0\left(\frac{V}{V_0}\right)^q \tag{6}$$

The q is considered the volume-based Gruneisen parameter $q = dln\gamma/dlnV$(Stixrude and Lithgow-Bertelloni, 2005).

E_{th} is defined as vibrational energy can be derived from the Debye model for a given volume and temperature as:

$$E_{th} = \frac{9nRT}{(\theta/T)^3}\int_0^{\theta/T}\frac{X^3 dx}{e^x - 1} \tag{7}$$

Where $\frac{3}{(\theta/T)^3}\int_0^{\theta/T}\frac{X^3 dx}{e^x - 1}$ is expressed the Debye function, and θ the Debye temperature.

while R is the gas constant. n represents the number of atoms per formula unit. When the difference between isothermal and isentropic values is taken into account, the isentropic bulk modulus as a function of temperature and pressure is given by:

$$K = K_T(1 + \alpha\gamma T) \tag{8}$$

Where αexpresses the thermal expansion factor as:

$$\alpha = \gamma C_V / K_T V \tag{9}$$

Where

$$K_T(V,T) = K_0(1+2f)^{5/2}\left[1 + \left(3K'_0 - 5\right)f + 27/2\left(K'_0 - 4\right)f^2\right] +$$

$$(\gamma/V)(\gamma + 1 - q)E_{th}(V,T) - \left(\gamma^2/V\right)$$

$$\left(TC_{V(V,T)} - 300C_{V(V,300K)}\right) \tag{10}$$

which is consistent with the expression to the third order obtained from an entirely isotropic thermodynamic analysis (Stixrude and Lithgow-Bertelloni, 2005).

C_v stands for the heat capacity at constant volume.

$$C_V = (dE_{th}/dT)_V = 4E_{th}/T - 9nR(\theta/T)/[exp(\theta/T) - 1] \tag{11}$$

θ denotes the Debye temperature, which is given as:

$$\theta = \theta_0 exp\left(\frac{\gamma_0 - \gamma(V)}{q}\right) \tag{12}$$

In formula number (10), the K'_0 represents the pressure derivative of the bulk modulus k_0 and f as:

$$f = \frac{1}{2}\left[\left(\frac{V_0}{V}\right)^{2/3} - 1\right] \tag{13}$$

The following equations describe how the shear modulus changes with temperature and pressure:

$$G(V,T) = (1+2f)^{5/2}\left[G_0 + \left(3K_0G'_0 - 5G_0\right)f + \left(6K_0G'_0 - 24K_0 - 14G_0 + \tfrac{9}{2}K_0K'_0\right)f^2\right] - \eta_s\tfrac{E_{th}(V,T) - E_{th}(V,T_0)}{V} \tag{14}$$

G'_0 is expressed the pressure derivative of the shear modulus G_0.

η represents the shear strain derivative of λ (Stixrude and Lithgow-Bertelloni, 2005).

$$\eta_s = \eta_{s0}\left(\frac{V}{V_0}\right) \tag{15}$$

The density is calculated by dividing the molar mass (m) by the molar volume to obtain the density as a function of temperature and pressure (V):

$$\rho = \left(\frac{m}{V}\right) \tag{16}$$

2.3. Algorithm and parameters of the gravity inversion

Herein, the 3D inversion method in the spherical coordinates was used (Liang et al., 2014, 2019) to facilitate the study of large regions. The study area extended between 25 degrees (20°E–45°E) in the longitude and 25 degrees (20°N–45°N) in the latitude. The gravity data of the investigated region were acquired collectively from GRACE and GOCE satellites with resolution (1° × 1°). Their density model was demonstrated in the same horizontal grid of 1° × 1° with a step every 50 km in depths. Using the seismic tomography model, the initial density model was performed in the inversion step of gravity data according to Li and Oldenburg (1998). The initial density model constrained the inversion results. The inversion objective function (ϕ) can be defined by the following Eq. (17):

$$\phi = \phi_d + \mu\phi_\rho \tag{17}$$

where the term ϕ_d denotes the data misfit function and ϕ_ρ represents the model objective function, and the regularization parameter is represented by μ that controls the balancing between two objective functions.

The two objective functions are denoted as follows:

$$\phi_d = \left\|K\rho - d_g\right\|_2^2, \text{and } \phi_\rho = \left\|W_\rho(\rho - \rho_{ini})\right\|_2^2 \tag{18}$$

where K denotes the integral operator used to transform the density into a gravity anomaly.d_g is the mantle gravity anomaly, ρ is the pending density vector, ρ_{ini} is the initial density vector, and W_ρ is the weighting

matrix in spherical coordinates (Liang et al., 2014) used in the model objective function as a very significant parameter.

2.4. Initial 3-D density model

Seismic S-wave velocities perturbations (Fig. 3) were converted to density perturbations according to the tomography model SL2013sv of Schaeffer and Lebedev (2013) to constrain the initial density model (Fig. 4). The initial density perturbations were computed at depths of 50, 100, 150, 200, 300, and 350 km, as demonstrated in Fig. 4. These density perturbations were converted from the initial temperature, which was transformed from S-wave velocities as used in Kaban et al. (2016a, 2016b). The low velocity is presented in the upper mantle below the Levant basin in the Mediterranean Sea, central Turkey, the Dead Sea Fault system, and the northern Red Sea at a depth of 50 km, relative to that of central Turkey (Gök et al., 2007; Meier et al., 2004). Those of lower velocity may be due to serpentinized mantle (Luccio and Pasyanos, 2007) and as interpreted in other subduction zones because of hydrothermal alteration where the existence of hydrous minerals such as serpentine could reduce the seismic velocity (Hyndman and Peacock, 2003). It spans beneath the mentioned regions at depths of 100 km (Fig. 3b).

The higher velocity could be due to peridotite or eclogite in the upper mantle if the crust is not oceanic beneath the lithosphere with a depth of ~150 km (Di Luccio and Pasyanos, 2007). There is an overall decrease in the mantle at depths 200 km from west to east beneath the regions around Cyprus and Crete, particularly toward northern and western directions (Fig. 3d), northern Aegean and the North Anatolian Fault, and the Dead Sea Fault System that are subjected to lower velocity. It is apparent in the models that a constant velocity was observed in the mantle beneath the Aegean region, Turkey, and central EMS at depths from 200 km to 300 km (Fig. 3b-e).

2.5. Relation between calculated Density Variations and Seismic Velocities

The compositional and thermal variations are considered the main factors affecting the upper mantle's density anomalies. They can be calculated from the conversion factor based on the relationship between the S-wave velocity perturbations and inverted density anomalies (Root et al., 2017). The conversion factor is clarified as follows:

$$p = (d\rho/\rho)/(dV_s/V_S) \tag{19}$$

where $d\rho$ represents the inverted density while ρ denotes the reference density shown in Table 1. The S-wave velocity perturbation is clarified by the ratio dV_s/V_s obtained from the tomography model SL2013sv (Schaeffer and Lebedev, 2013). The thermal and compositional variations affect the inverted density in the upper mantle according to the conversion factor. Temperature dominates the inverted density if the conversion factor is positive, while composition determines the density variations if the conversion factor has a negative value.

3. Inversion results

This work is based on low and high density seismic tomography observations to understand the tectonics of the EMS, which has become a vital tool in connecting tectonics and mantle geodynamics. The RMGA causes evident variations between the inverted and initial density models. In comparing the initial and inverted models, the initial model gives negative density anomalies at a depth of 100 and 150 km beneath Cyprus (Fig. 4b,c). In contrast, the inverted one shows a high positive density anomaly at the same depths (Fig. 5b, c). By applying the method of Liang et al. (2014), we can get more details unavailable from seismic data. The inverted density anomaly describes the lateral compositional and thermal variations in the lithosphere that help to understand the tectonic evolution under the Mediterranean Sea and the adjacent regions (Fig. 5).

High-density anomaly covers the lithosphere beneath the Mediterranean Sea and surrounding regions, but it varies from the Levant basin to the Pliny and Strabo trenches at 100 km. The maximum values are distributed in the continental zones, mainly beneath the northeast of the Arabian plate toward the south and Cyprus at depths from 150 km to 300 km. An apparent decrease in the density is noticed at depths between 300 and 350 km beneath the northern part of the Red Sea at Aqaba Gulf and the Suez Gulf. The low-density anomaly dominates the upper mantle beneath the Pliny and the Strabo trenches and south of the Aegean Sea below 100 km (Fig. 5b). The high-density anomaly thickens eastwards or westwards, covers the Mediterranean Sea downwards, then decreases at depths 300 km (Fig. 5e). The density in the deeper mantle seems not to have changed beneath Syria and Lebanon's coasts at depths of 150 and 200 km (Fig. 5c, d). The low-density zone thickens under the Red Sea. It controls the depth from 300 to 350 km (Fig. 5e, f), resultant of the variation of compositional and thermal anomalies, as compared to high-density zones (Fig. 5). The inverted density anomaly emphasizes that low density beneath the upper mantle in the collision zones and plate boundaries, which indicates that higher temperature dominates. The density structure is predicted according to the model (Table 1), which indicates the density increment with depth (but not always, as its increment is based on the anomaly in amplitude as well).

4. Discussion

4.1. The Mediterranean Sea

The EMS is considered an ideal location to study the relationship between the sub-surface and upper mantle geodynamics. The high-density and low-density zones appear at different depths. High density controls the upper mantle at a depth of 100 km that causes the positive anomaly of the RMGA beneath the Levant basin in the EMS (Fig. 5b). The low-density zone covers the western parts of the Levant basin toward the Eratosthenes seamount at a depth of 200 km (Fig. 5d). The extension of low and high-density zone differs from that in the west. This appears from gravity anomalies of the RMGA in the Mediterranean Sea. The thinnest layer of the high-density zone is located in the oceanic upper mantle beneath southwest EMS. This discrepancy in density values of the mantle lithosphere leads to the exceptional nature of the EMS lithospheric structure. The older oceanic lithosphere beneath the Levant basin is described as high density in the southern Mediterranean Sea. It continues with Seafloor spreading of the Red Sea, which has been cooling down since ~80 Ma (Segev et al., 2006).

The high density in the inverted density model is caused by a stagnated slab of the Mediterranean Sea beneath the Cyprus trench (Figs. 5a-f). On the other hand, this slab does not appear in the deep layers beneath other trenches (Fig. 6). The relatively high density in the uppermost mantle extends from the EMS to the continental Arabian plate, which is found beneath Cyprus and the Levant basin in the cross sections of CC1, EE1and DD1 along WE (Fig. 6). Even though the thickness of the sedimentary layer in the Arabian plates and southern Turkey is quite shallow and roughly 3–5 km under the DSFS (Di, 2007), the subduction might be impacted by sediments (Behr et al. 2018; Erdős et al., 2021) and fluids produced by dewatering processes (Vannucchi et al., 2012; Erdős et al., 2021) over an extended period of time. The impact of sediments on subduction beyond its thickness is currently being disputed.The Mediterranean Sea undergoes subduction that might initiate from the Hellenic Trench. This might be due to its broken part in the upper mantle, which is caused by the upwelling magma from the melting asthenosphere, particularly underneath the Eratosthenes seamount (Figs. 6D, J). The upper mantle upwelling heats the lower lithosphere and causes the melting. This replaces the cold materials in the Mediterranean Sea. Mantle convection plays a significant role in forming all geological features on the surface. Many seismic studies have

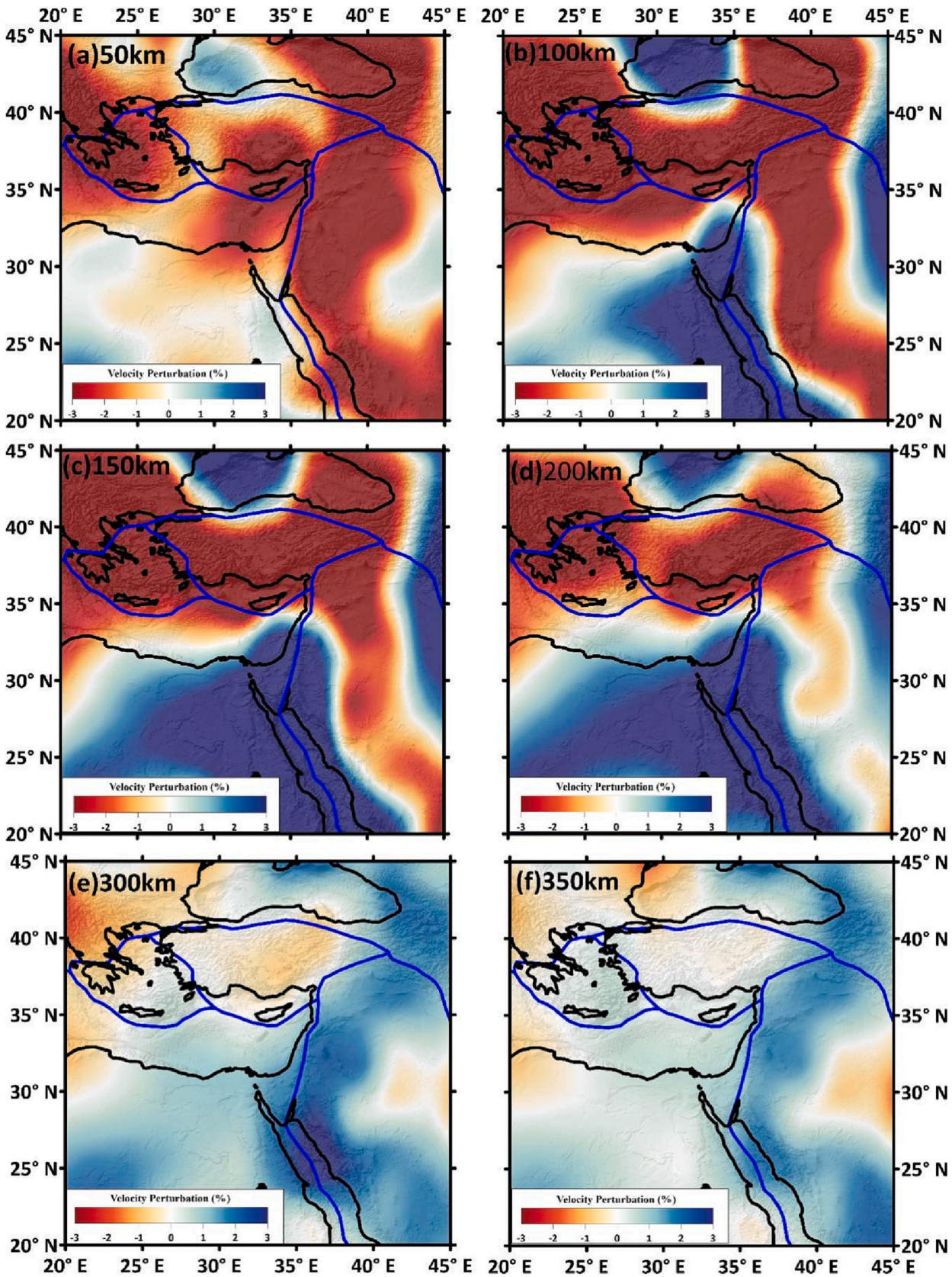

Fig. 3. S-wave velocity perturbations of the tomography model SL2013sv of Schaeffer and Lebedev (2013) at the depths 50, 100, 150, 200, 300, and 350 km.

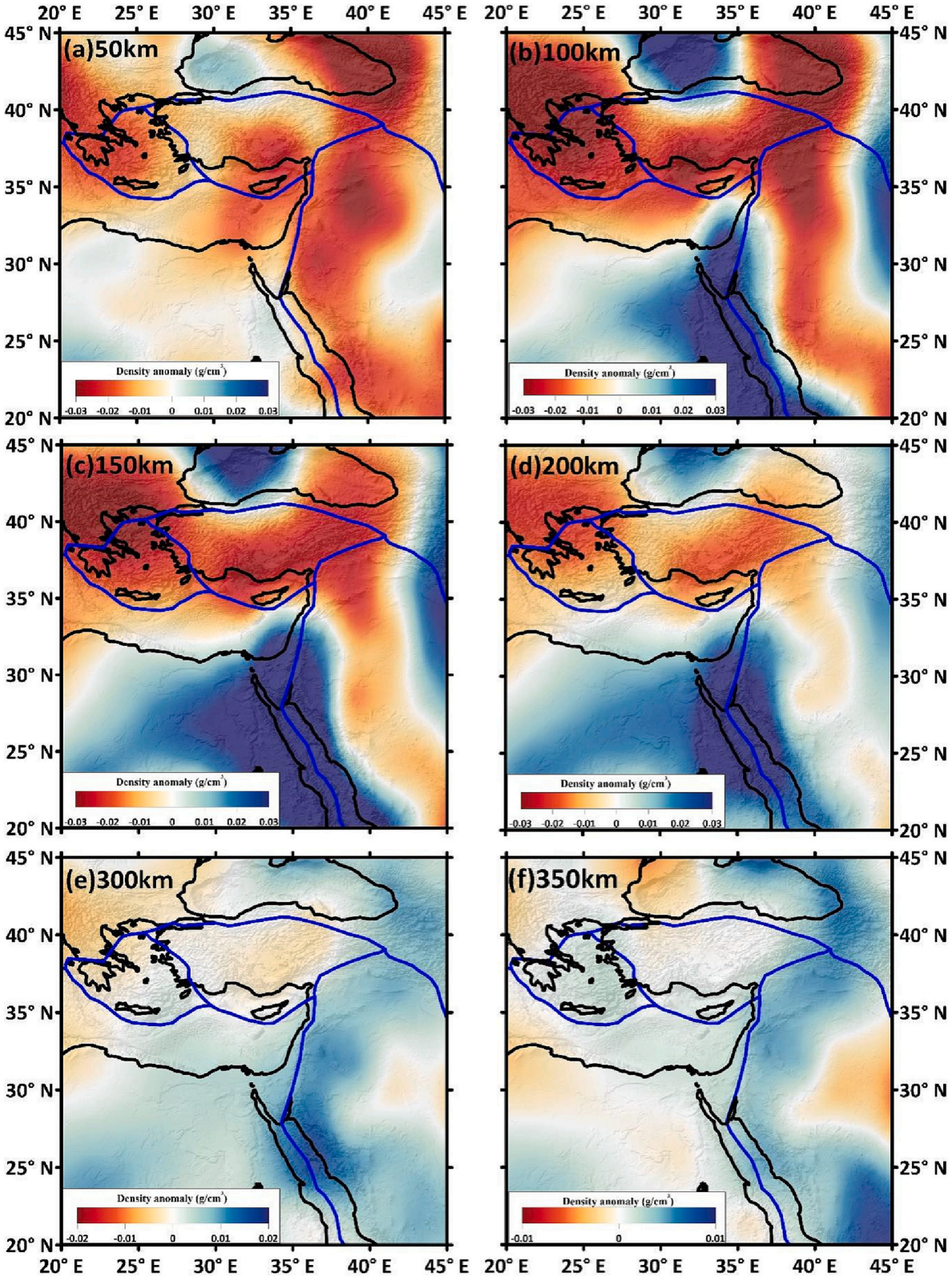

Fig. 4. The initial density model at the depths 50, 100, 150, 200, 300, and 350 km. Black lines represent plate boundaries.

determined this phenomenon of subduction trench (Harash and Chen, 2022; Welford et al., 2015; Robertson, 1998). However, the subduction is not visible in the inverted density models of the upper mantle (Fig. 6). It is apparent in other models beneath the Eratosthenes seamount due to better data resolution. (Figs. 6A-L). The profile JJ1 captures the high-density anomaly in Fig. 6J, caused by an elevated mantle lithosphere beneath the Eratosthenes as a dense bulk in the lithosphere. This leads to a compressional push-up mechanism for the seamount. The thickest low-density layer beneath the Mediterranean Sea is associated with the Red Sea spreading during 50 Ma. Therefore, the asthenosphere upwelling caused the low-density materials by the delaminated slab. The low velocities are related to the lower crust beneath the Levant basin

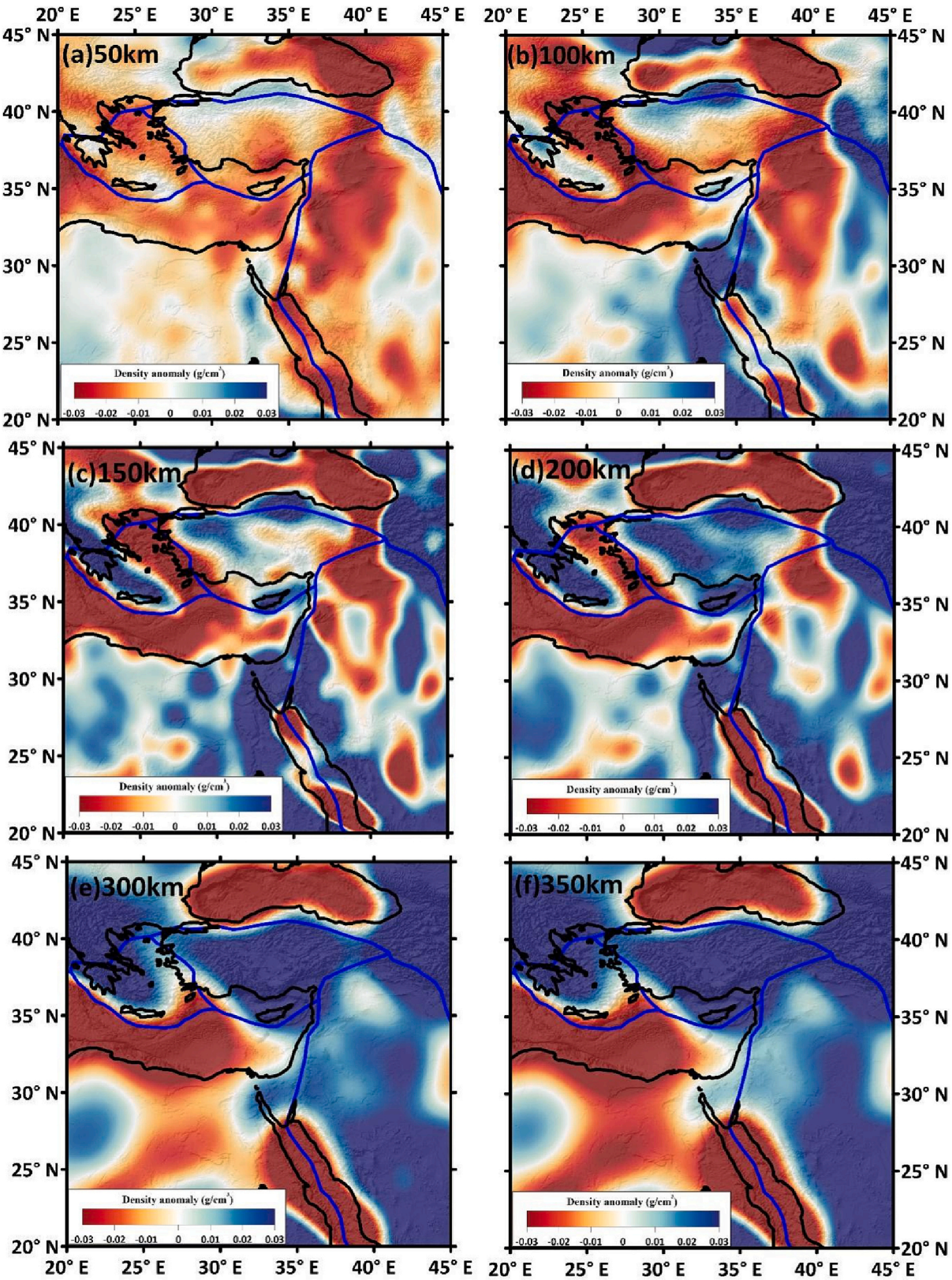

Fig. 5. Inverted density variations at the depths 50, 100, 150, 200, 300 and 350 km. Black lines represent plate boundaries.

(Fig. 3). In the lower lithosphere, seismic velocity increase with depth to about 150 km. At the same time, partial melting and sedimentation control the velocity in the upper mantle (Ben-Avraham et al., 2002a, 2002b).

It is noticed along profile JJ1 that an apparent density anomaly of the Eratosthenes Seamount extends for about 400 km (Fig. 6J). The seamount is considered a bulky sub-rectangular northward continental part, separated from the African plate (Harash et al., 2022; Ben-Avraham et al., 2002b; Netzeband et al., 2006), which raised feature in the EMS besides the Levant basin and Cyprus. It was uplifted due to the

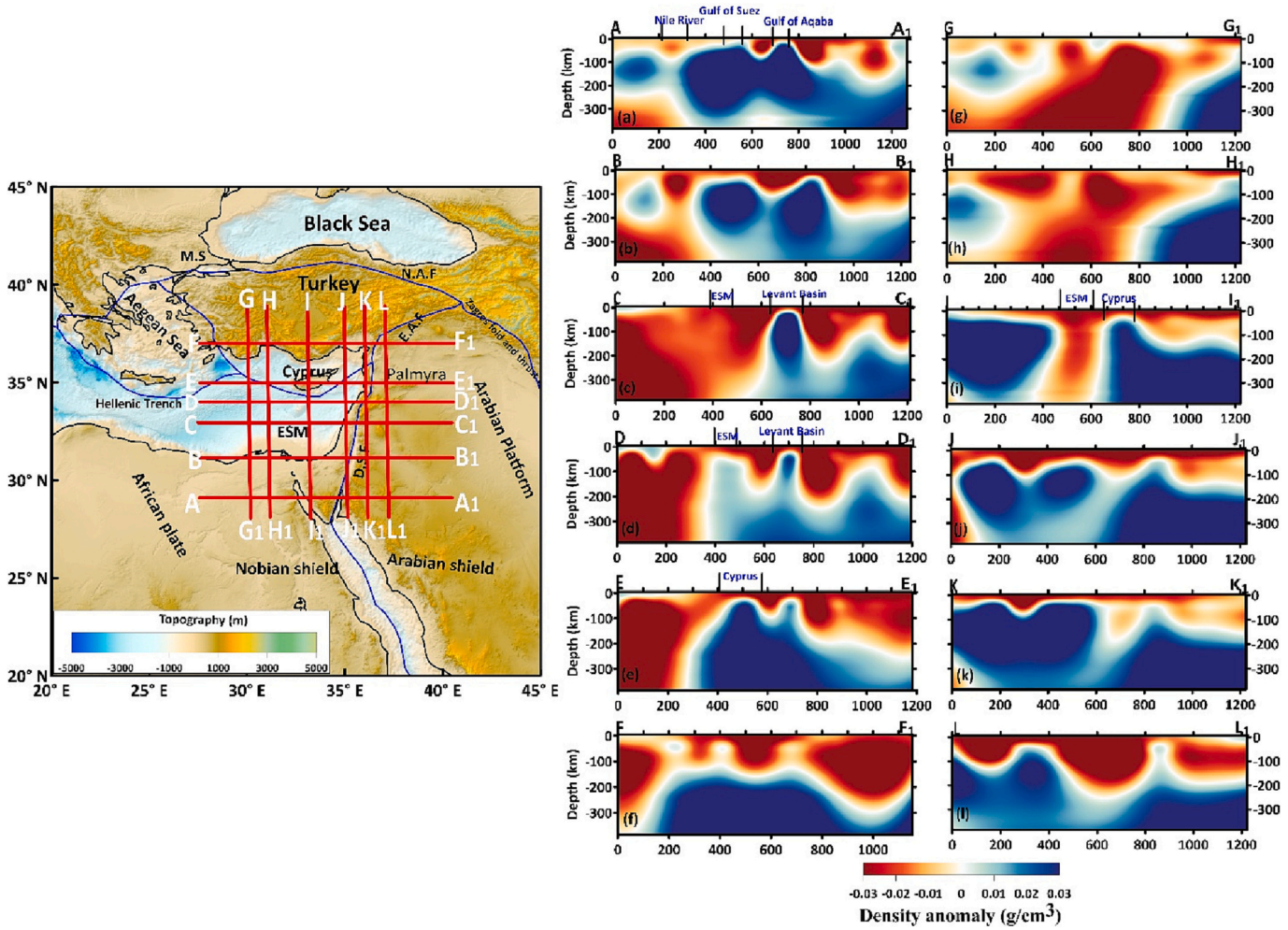

Fig. 6. Vertical profiles of the inverted density structure: (a) AA_1, (b) BB_1, (c) CC_1, (d) DD_1, (e) EE_1, (f) FF_1, (g) GG_1, (h) HH_1, (i) II_1, (j) JJ_1, (k) KK_1, (l) LL_1.

collision of the Eratosthenes Seamount with Cyprus toward the northern part during the early Miocene time (Harash et al., 2022; Robertson, 1998). Robertson et al. (1998) suggested that the main reason for the uplifted seamount is the effects of regional tectonic upwarping. It is related to the northern subduction origination of the remnant of Neotethys oceanic crust in the Mediterranean Sea. In the late Pliocene to early Pleistocene, the crust thickened over the African Plate's subduction below Eurasia. At the same time, before ~30–35 Ma, the mantle upwelled to initiate the first step to generate the EMS that invaded the subduction trench along the Cyprus Arc, which might lead to slab breakoff of the Eratosthenes Seamount (Feld et al., 2017). As these slabs moved backward to the Eurasian top plate during plate convergence, the asthenosphere began to flow backward in the direction of the subduction zones. The slab destruction could cause trench migration (Faccenna et al., 2014). This flow comes from the back arc and could be located far from the subduction zones and is currently represented beneath the Eratosthenes Seamount.

Dehydration of the subduction slab might be the reason for the above phenomenon (Arcay et al., 2006). This interpretation is in agreement with the results of Welford et al. (2015), who considered EMS as an older magmatic intrusion since the high seismic velocity in the southwestern direction of EMS (Fig. 3). At the same time, the Troodos ophiolite was uplifted and caused the high-density anomaly beneath the Eratosthenes Seamount. A great high-density block in the southern Cyprus region appears at a depth of 100 km (Fig. 5b), and is a remnant of a subduction slab from the African plate at a depth of 200 km. There is a large area with low density at a depth of 100 km (Fig. 5b) beneath the western EMS, and this is due to low velocity supported by thermal effects that affect the density anomalies.

4.2. Adjacent plates

To better understand the tectonics in this complicated region, examining density differences in the upper mantle would supply a supplementary balance of the lithosphere. The density structure of the northern EMS varies from low-density asthenosphere, which is distinctive at all cross sections AA1, BB1, CC1, DD1, EE1, FF1, GG1, HH1, II1, JJ1, KK1, and LL1 that consist of an offshore part and an onshore part (Fig. 6). The 125 km thick density beneath the old oceanic upper mantle. The density structure associated with tomography models with a good result between 100 and 150 km (Fig. 5b, c). The low-density layers extend beneath the adjacent regions of the Mediterranean Sea and the northern and eastern parts that extend over the two plates. High upper-mantle density is observed in the southeastern Mediterranean beneath the Gulf of Suez and Gulf of Aqaba, as shown in profile AA1 (Fig. 6A). The profile LL1 (Fig. 6L) runs from Turkey in the north through eastward of the dead sea fault to the south showing low upper mantle density in this part of the Arabian plate (Fig. 6).

In general, the upper mantle density variations are due to the tectonic distribution of the region. The low-density anomalies are located beneath the Gulf of Eden and the Red Sea spreading zone, especially at their intersection (Fig. 5). The maximum density values correspond with the continental regions, especially toward the northeast of the Arabian Plate. These results agree with Ebbing (2006) in a similar study area. A

high-density value could be caused by active tectonics, which results in the dynamic forces in the upper mantle, especially beneath the Levant basin (Fig. 6C). There are obvious variations in the mantle structure between the Arabian shield and the platform, particularly in the southern part as it is denser than the Arabian shield. These results agree with other models (Schaeffer and Lebedev, 2013; Koulakov, 2011).

The density variation of the upper mantle and asthenosphere beneath the Mediterranean Sea is affected by the northwestern subduction zone. The reason for these variations is the composition differences in the upper mantle. The inverted density models determine the subduction zone shape (Fig. 6). High density controls another large area beneath the Arabian shield and its platform at a depth of 200 km (Fig. 5d). The density structure has no big difference in some areas because of their tectonic evolution. Moreover, the crust varies beneath the Mediterranean Sea, where it shows higher thickness in the south direction from the Levant basin toward the Eratosthenes seamount, about 27 km, whereas 33 km under Cyprus and 38–40 km toward the continent (Di Luccio and Pasyanos, 2007; Khair and Tsokas, 1999). In addition, the nature of the crust also varies beneath ESM as it is considered a continent crust (Ben-Avraham et al., 2002a, 2002b; Di Luccio and Pasyanos, 2007).

4.3. Density–velocity conversion factor and its relation to tectonics

The conversion factor represents the compositional and thermal effects that influence density anomaly in the lithosphere. It is based on the relationship of the density–velocity perturbation. Fig. 7 presents the estimated conversion factor between the S-wave velocity perturbation and initial density anomalies from initial temperature, as used in Kaban et al. (2016a, 2016b). The density anomalies in the upper mantle and lower layers beneath the Mediterranean Sea, particularly the Levant basin at depths of 85 km – 95 km (Fig. 7 e,f), Cyprus at depths of 55 km – 65 km (Fig. 7 b,c), and the area located in the NW corner, with a NW-SE direction covering Greece and Crete, and a small anomaly in the NE corner, near the Black Sea are dominated by compositional effects according to the negative conversion factor (Fig. 7 a-f). However, other areas like Eratosthenes seamount, middle of the Arabian shield, and other regions, between plates are dominated by thermal effects along the subduction zones at the plate margins. It is shown that the upper mantle structure beneath the Mediterranean Sea is different from the surrounding region according to the conversion factor variation on the vertical and lateral sides (Fig. 7e-f). The conversion factor is negative beneath the Nubian shield close to Red Sea and Lattakia ridge in the eastern part of Cyprus at depths between 85 km and 95 km (Fig. 7 e,f), which indicates it is dominated by the compositional effect related to dense mantle materials below the Mediterranean Sea. However, it differs from other parts dominated by thermal effects.

4.4. Tectonic activity of the Eratosthenes Seamount

It is assumed that the Eratosthenes Seamount is a part of a continent that splitted off the northern edge of the North African plate in the early Mesozoic (Robertson, 1998; Wen et al., 2021), during the stage of seamount development as shown (Fig. 8a). During the Messinian period, the Eratosthenes Seamount was eroded. Additionally, Messinian-folding deformation of the ESM may have started during that time, and this deformation is likely to be due to the faulting of pre-Pliocene-Pleistocene originally (Robertson et al., 1998), and dispersed elastic flow in the upper-mantle leads to deformation conversion from crisp to elastic with temperature increment (Hirth and Kohlstedt, 2003; Barbot and Weiss, 2021).The Pliocene and Quaternary saw the majority of the folding deformation in this region (Gao et al., 2020). The ESM changed from an isolated platform to the current dome-shaped high due to continuous folding deformation, which is considered as a volcanic block that has been found at the continental margin of Africa- Arabian plates during the early Mesozoic rifting (Fig. 8a).

On the eastern edge of the ESM, the folding deformation created a little flatland area that is covered in Messinian salt. The tectonic evolution of the Eratosthenes Seamount has experienced subduction, collision, and post-collision stages. As being it is constructed due to the subduction, it is still active undergoing tectonic collision with Cyprus (Robertson, 1998; Galindo-Zaldívar et al., 2001). Eratosthenes Seamount is accompanied by deeper magmatic intrusions staggered by the African plate's thinner continental crust south of Cyprus then then start to thicken close to Cyprus Arc because of continental collision at the beginning of the Miocene (Robertson et al., 1998; Galindo-Zaldívar et al., 2001).

The collision is considered an interruption to the Africa-Anatolia convergence south of Cyprus, caused by the arrival of the relatively thick and buoyant Eratosthenes block to its present location south of Cyprus in Holocene time (Fig. 8c). The new location of Eratosthenes seamount is interrupted as result of convergence between Africa and Anatolia plates during the Late Cretaceous and early Tertiary period (Kempler, 1998).

There is a lot of basalts belongs to Triassic period in the southern edge of Turkey and on the Cyprus Island northern of the ESM (Robertson Alastair, 1998), the tectonic activity including faults and magma explosion are spread at the levant edges, so the Jurassic thickness has thickened more than 3 km on the levant margin (Garfunkel, 2004), in which lead to forming horst blocks like Eratosthenes seamount with area of 8750 km^2 roughly, which splitted from the Afra-Arabia plate(Garfunkel, 1998; Eppelbaum and Katz, 2015). In the late Miocene, subduction of the Arab- the Eurasian Plates detached (Hinsbergen, 2010), and the continent-continent collision stage between Eratosthenes and Cyprus Arc started as shown (Fig. 8b).

During Pliocene and Quaternary periods, the ESM has been deformed a lot as many faults and folds has been formed due to collision at that time (Fig. 8c). There are some potential causes stop behand the Eratosthenes Seamount formation and the destruction of plate boundary in the northward direction during the Miocene period. There was a subduction before this period and this subduction was unsteady and later broke off, thus in that case lead to experience the overlaying plate an uplift (Robertson et al., 1998; Fig. 8d). Uplift could be a result of accumulated compression in the direction of subduction southern Cyprus that was attributed due to the Eratosthenes Seamount – Cyprus collision in the southward direction of Cyprus after the subduction stage (Mart et al., 1997; Fig. 8c). As a result, the Slab regress still play a significant control on the geodynamics of the Eastern Mediterranean, providing a pull force for Aegean extension and Anatolian extrusion too. The subduction and collision that occurs along with trench regress is a good explanation for this backarc rifting (Barbot and Weiss, 2021).

5. Conclusions

A 3D density structure of the lithosphere and upper mantle beneath the EMS and the adjacent region was constructed based on gravity inversion constrained by a seismic tomography model. Many essential features have been noticed in the EMS region's upper mantle, especially beneath the ESM. Results show that the deep structure under the Eratosthenes seamount in the Mediterranean Sea is the source of the intensity and genesis of tectonic activity. Therefore, the convergence region of two low-density anomaly zones (Africa-Anatolia) may be interpreted as a significant tectonic unit (Eratosthenes seamount) caused by the arrival of the relatively thick and buoyant Eratosthenes block to its present location south of Cyprus in Holocene time based on the density model interpretation beneath the Mediterranean Sea during the Late Cretaceous and early Tertiary period.The low-density upper mantle is distributed on the western side of the Mediterranean Sea. In contrast, the eastern parts of the Mediterranean Sea are dominated by high density related to the old lithosphere. The comparison between density and seismic models revealed that some characteristics were not shown in both. The thin, dense and cold layer is located in the lithosphere beneath

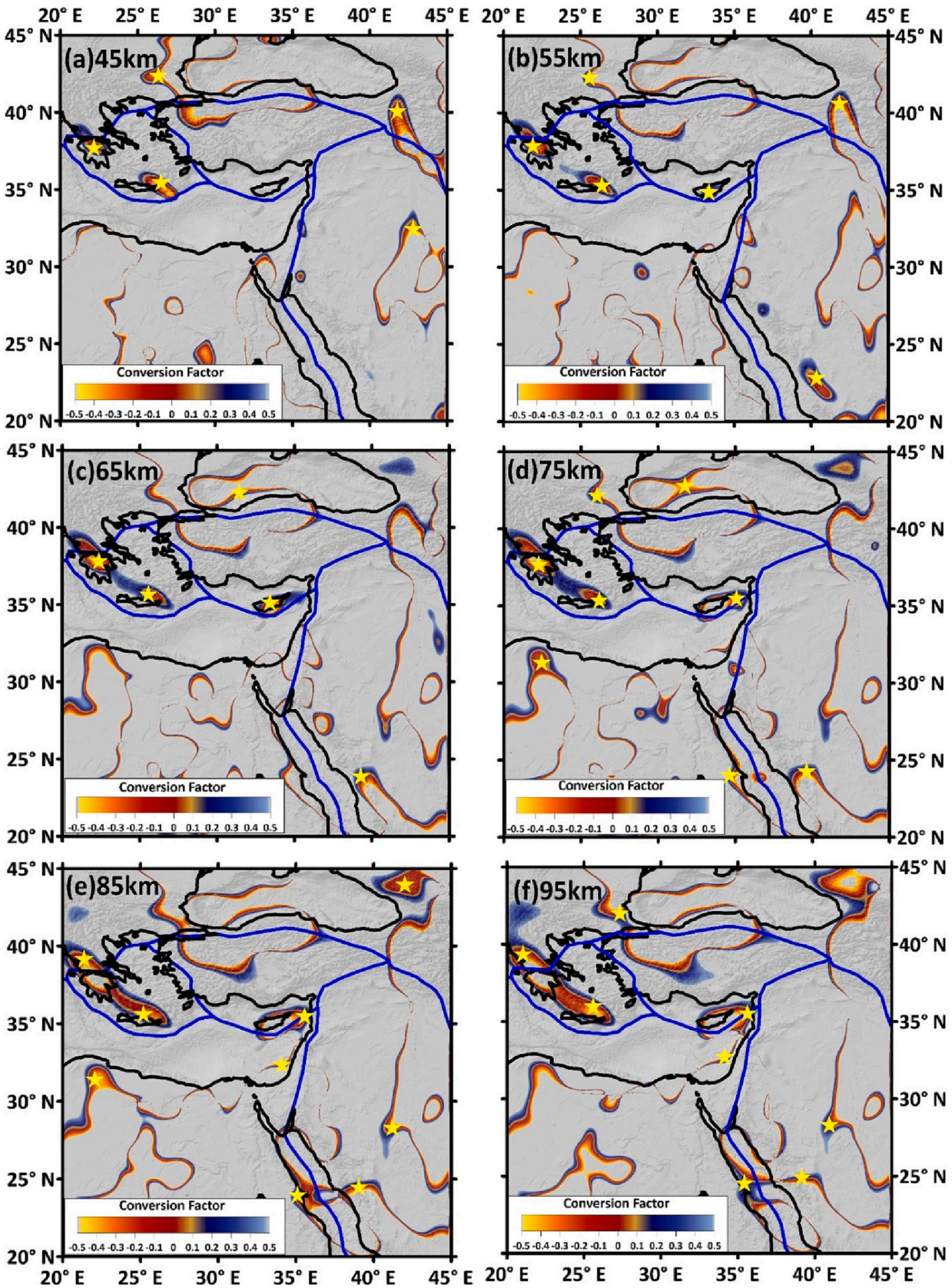

Fig. 7. The lateral distribution of the conversion factor between the S-wave velocity perturbations (SL2013sv) and our final density anomalies at depths ranging between 45 and 95 km. yellow stars refer to Compositional effect. (For interpretation of the references to colour in this figure legend, the reader is referred to the web version of this article.)

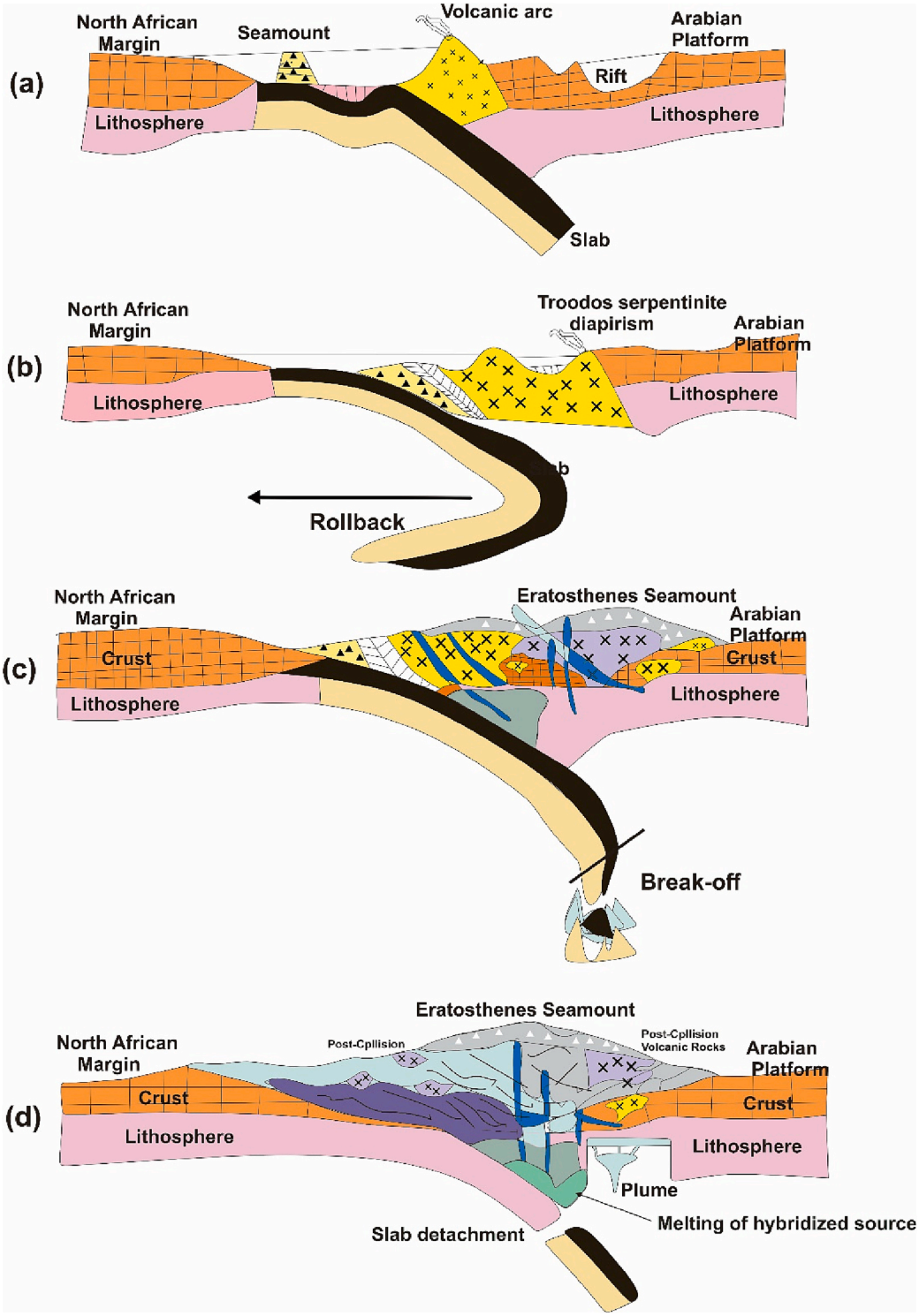

Fig. 8. Tectonic evolution of the Eratosthenes Seamount in Eastern Mediterranean, (a) Subduction of the Seamount, (b) Pre-Collision of the Seamount, (c) Collision Stage and (d) Post-Collision Stage, modified after Dilek and Sandvol (2009).

the west ESM, whereas the thick, soft, and low-density layer is located below the lithosphere and might be linked to the asthenosphere in the region from west to east at a depth of 100 km. At a depth of 150 km, there is a transition zone extending from negative-density anomalies to positive anomalies below the Mediterranean Sea and the Red Sea. The subduction zone plays a significant role in the density transition because of interaction with the asthenosphere. The results of the inverted density model show high density at depths of 200–300 km beneath the Mediterranean Sea according to their density structure. However, according to the negative conversion factor, the compositional variations affect the density structure more than the thermal ones.

CRediT authorship contribution statement

Fayez Harash: Conceptualization, Methodology, Software, Data curation, Writing – original draft, Writing – review & editing. **Chao**

Chen: Supervision. **Qing Liang:** Conceptualization, Methodology, Software. **Chenming Tu:** Conceptualization, Methodology, Software, Data curation, Writing – original draft. **Nadhir Al-Ansari:** Visualization, Investigation, Software, Validation. **Khalaf Amin:** Software, Validation. **Imad ALrawi:** Writing – review & editing. **Aref ALshameri:** Data curation, Writing – original draft, Visualization, Investigation.

Funding

The publication fees were paid gratefully by Lulea University of Technology (Sweden). This work was supported by Natural Science Foundation of China (Nos. 42174090 and 41604060), the MOST Special Fund from the State Key Laboratory of Geological Processes and Mineral Resources (MSFGPMR2022-4), China University of Geosciences.

Declaration of Competing Interest

The authors declare no conflict of interest.

Data availability

The datasets used and/or analysed during the current study available from the corresponding author on reasonable request.

References

Agrawal, M., Pulliam, J., Sen, M.K., Dutta, U., Pasyanos, M.E., Mellors, R., 2015. Crustal and uppermost mantle structure in the Middle East: assessing constraints provided by jointly modelling Ps and Sp receiver functions and Rayleigh wave group velocity dispersion curves. Geophys. J. Int. 201 (2), 783–810. https://doi.org/10.1093/gji/ggv050.

Arcay, D., Doin, M.P., Tric, E., Bousquet, R., de Capitani, C., 2006. Overriding plate thinning in subduction zones: Localized convection induced by slab dehydration. Geochem. Geophys. Geosyst. 7, Q02007. https://doi.org/10.1029/2005GC001061.

Barazangi, M., Seber, D., Chaimov, T., Best, J., Litak, R., Al-Saad, D., Sawaf, T., 1993. Tectonic evolution of the Northern Arabian Plate in Western Syria. In: Recent Evolution and Seismicity of the Mediterranean Region, 117–140. https://doi.org/10.1007/978-94-011-2016-6_5.

Barbot, S., Weiss, J.R., 2021. Connecting subduction, extension and shear localization across the Aegean Sea and Anatolia. https://doi.org/10.1093/gji/ggab078.

Ben-Avraham, Z., 1985. Structural framework of the Gulf of Elat (Aqaba), northern Red Sea. J. Geophys. Res. 90 (B1), 703–726. https://doi.org/10.1029/JB090iB01p00703.

Ben-Avraham, Zvi, Ginzburg, A., Makris, J., Eppelbaum, L., 2002a. Crustal structure of the Levant Basin, eastern Mediterranean. Tectonophysics 346, 23–43. https://doi.org/10.1016/S0040-1951(01)00226-8.

Ben-Avraham, Zvi, Ginzburg, A., Makris, J., Eppelbaum, L., 2002b. Crustal structure of the Levant Basin, eastern Mediterranean. Tectonophysics 346 (1–2), 23–43. https://doi.org/10.1016/S0040-1951(01)00226-8.

Berk Biryol, C., Beck, S.L., Zandt, G., Özacar, A.A., 2011. Segmented African lithosphere beneath the Anatolian region inferred from teleseismic P-wave tomography. Geophys. J. Int. 184 (3), 1037–1057. https://doi.org/10.1111/j.1365-246X.2010.04910.x.

Brew, G., Best, J., Barazangi, M., Sawaf, T., 2003. Tectonic evolution of the NE Palmyride mountain belt, Syria: the Bishri crustal block. J. Geol. Soc. 160 (5), 677–685. https://doi.org/10.1144/0016-764902-161.

Cammarano, F., Goes, S., Vacher, P., Giardini, D., 2003. Inferring upper-mantle temperatures from seismic velocities. Phys. Earth Planet. Inter. 138, 197–222. https://doi.org/10.1016/S00319201(03)00156-0.

Chaves, C.A.M., Ussami, N., 2013. Modeling 3-D density distribution in the mantle from inversion of geoid anomalies: Application to the Yellowstone Province. J. Geophys. Res. Solid Earth 118 (12), 6328–6351. https://doi.org/10.1002/2013JB010168.

Di Luccio, F., Pasyanos, M.E., 2007. Crustal and Upper-Mantle Structure in the Eastern Mediterranean from the Analysis of Surface Wave Dispersion Curves, pp. 1139–1152. https://doi.org/10.1111/j.1365-246X.2007.03332.x.

Dilek, Y., Sandvol, E., 2009. Seismic structure, crustal architecture and tectonic evolution of the Anatolian-African Plate Boundary and the Cenozoic Orogenic Belts in the Eastern Mediterranean Region. Geol. Soc. Spec. Publ. 327 (March 2014), 127–160. https://doi.org/10.1144/SP327.8.

Ebbing, 2006. The lithospheric density structure of the Eastern Alps. Tectonophysics 414, 145–155. https://doi.org/10.1016/j.tecto.2005.10.015.

Erdős, Z., Huismans, R.S., Faccenna, C., Wolf, S.G., 2021. The Role of Subduction Interface and Upper Plate Strength on Back-Arc Extension: Application to Mediterranean Back-Arc Basins. Tectonics 40 (8). https://doi.org/10.1029/2021TC006795.

Faccenna, C., Becker, T.W., Auer, L., Billi, A., Boschi, L., Brun, J.P., Serpelloni, E., 2014. Reviews of Geophysics Mantle dynamics in the Mediterranean. Rev. Geophys. 52 (3), 283–332. https://doi.org/10.1002/2013RG000444.

Feld, C., Mechie, J., Hübscher, C., Hall, J., Nicolaides, S., Gurbuz, C., Weber, M., 2017. Crustal structure of the Eratosthenes Seamount, Cyprus and S. Turkey from an amphibian wide-angle seismic profile. Tectonophysics 700–701, 32–59. https://doi.org/10.1016/j.tecto.2017.02.003.

Flerit, F., Armijo, R., King, G., Meyer, B., 2004. The mechanical interaction between the propagating North Anatolian Fault and the back-arc extension in the Aegean. Earth Planet. Sci. Lett. 224, 347–362. https://doi.org/10.1016/j. epsl.2004.05.028.

Förste, C., Bruinsma, S.L., Abrikosov, O., Lemoine, J.M., Marty, J.-C., Flechtner, F., Balmino, G., Barthelmes, F., Biancale, R., 2014. EIGEN-6C4 - the latest combined global gravity field model including GOCE data up to degree and order 2190 of GFZ Potsdam and GRGS Toulouse. GFZ Data Serv. https://doi.org/10.5880/icgem.2015.1.

Galindo-Zaldívar, J., Nieto, L.M., Robertson, A.H.F., Woodside, J.M., 2001. Recent tectonics of eratosthenes seamount: an example of seamount deformation during incipient continental collision. Geo-Mar. Lett. 20 (4), 233–242. https://doi.org/10.1007/s003670000059.

Gao, H., Wen, Z., Shi, B., Wang, Z., Song, C., 2020. Tectonic characteristics of the Eratosthenes Seamount and its periphery: Implications for evolution of the eastern Mediterranean. Mar. Geol. 428, 106266 https://doi.org/10.1016/j.margeo.2020.106266.

Garfunkel, Z., 1998. Constrains on the origin and history of the Eastern Mediterranean basin. Tectonophysics 298 (1–3), 5–35. https://doi.org/10.1016/S0040-1951(98)00176-0.

Gök, R., Pasyanos, M.E., Zor, E., 2007. Lithospheric structure of the continent-continent collision zone: Eastern Turkey. Geophys. J. Int. 169 (3), 1079–1088. https://doi.org/10.1111/j.1365-246X.2006.03288.x.

Harash, F., & Chen, C., 2022. Determination of curie point depth distribution and heat flow regime characteristics in Eratosthenes Seamount, Eastern Mediterranean Sea. Energies 15, 8634(Geothermal), 0–13. doi: https://doi.org/10.3390/en15228634.

Kaban, M.K., Schwintzer, P., 2001. Oceanic upper mantle structure from experimental scaling of Vs ad density at different depths. Geophys. J. Int. 147 (1), 199–214. https://doi.org/10.1046/j.0956-540X.2001.01520.x.

Kaban, M.K., Yuanda, T.R., 2014. Density Structure, Isostatic Balance and Tectonic Models of the Central Tien Shan. Surv. Geophys. 35 (6), 1375–1391. https://doi.org/10.1007/s10712-014-9298-7.

Kaban, M.K., Schwintzer, P., Reigber, C., 2004. A new isostatic model of the lithosphere and gravity field. J. Geod. 78, 368–385.

Kaban, M.K., Petrunin, A.G., Schmeling, H., Shahraki, M., 2014. Effect of Decoupling of Lithospheric Plates on the Observed Geoid. Surv. Geophys. 35 (6), 1361–1373. https://doi.org/10.1007/s10712-014-9281-3.

Kaban, M.K., Mooney, W.D., Petrunin, A.G., 2015. Cratonic root beneath North America shifted by basal drag from the convecting mantle. Nat. Geosci. 8 (10), 797–800. https://doi.org/10.1038/ngeo2525.

Hinsbergen, D.J.J., 2010. A key extensional metamorthic complex reviewed and restored: the Menderes Masif of western Turkey[J]. Earth Sci. Rev. 102, 60–76.

Hirth, G., Kohlstedt, D., 2003. Rheology of the uper mantle and the mantle wedge: a view from experimentalists. In: Eiler, J. (Ed.), Inside the Subduction Factory, Geophys. Monogr. Ser., 138. American Geophysical Union, Washington, DC, pp. 83–106.

Hyndman, R.D., Peacock, S.M., 2003. Serpentinization of the forearc mantle. Earth Planet. Sci. Lett. 212, 417–432.

Jackson, I, Rigden, S M, 1996. Analysis of P-V-T data; constraints on the thermoelastic properties of high-pressure minerals[J]. Phys. Earth Planet. Inter. 96, 85–112.

Kaban, M.K. (Ed.), 2011. Gravity anomalies, interpretation, in Encyclopedia of Solid Earth[M]. Geophysics, 2nd ed. Springer, Berlin, pp. 456–461.

Kaban, M.K., El Khrepy, S., Al-Arifi, N., Tesauro, M., Stolk, W., Kaban, M.K., 2016a. Three-dimensional density model of the upper mantle in the Middle East: Interaction of diverse tectonic processes. J. Geophys. Res. 5349–5364. https://doi.org/10.1002/2015JB012755.

Kaban, M.K., Stolk, W., Tesauro, M., El Khrepy, S., Al-Arifi, N., Beekman, F., Cloetingh, S. A.P.L., 2016b. 3D density model of the upper mantle of Asia based on inversion of gravity and seismic tomography data. Geochem. Geophys. Geosyst. 17 (11), 4457–4477. https://doi.org/10.1002/2016GC006458.

Kempler, D., 1998. Eratosthenes Seamount: the possible Spearhead of Incipient Continental Collision in the Eastern Mediterranean. Proc. Ocean Drilling Prog. Scientific Results 160, 709–721. Retrieved from. http://www-odp.tamu.edu/publications/160_SR/VOLUME/CHAPTERS/CHAP_53.PDF. Retrieved from.

Klimke, J., Ehrhardt, A., 2014. Impact and implications of the Afro-Eurasian collision south of Cyprus from reflection seismic data. Tectonophysics 626 (1), 105–119. https://doi.org/10.1016/j.tecto.2014.04.002.

Koulakov, I., 2011. High - frequency P and S velocity anomalies in the upper mantle beneath Asia from inversion of worldwide traveltime data. J. Geophys. Res. 116 (December 2010), 1–22. https://doi.org/10.1029/2010JB007938.

Lee, C.T., 2003. Compositional variation of density and seismic velocities in natural peridotites at STP conditions: Implications for seismic imaging of compositional heterogeneities in the upper mantle. J. Geophys. Res. 108 (B9), 2441. https://doi.org/10.1029/2003JB002413.

Li, Y., Oldenburg, D.W., 1998. 3-D inversion of gravity data. Geophysics 63 (1), 109–119. https://doi.org/10.1190/1.1444302.

Liang, Q., Chen, C., Li, Y., 2014. 3-D inversion of gravity data in spherical coordinates with application to the GRAIL data. J. Geophys. Res. E Planets 119 (6), 1359–1373. https://doi.org/10.1002/2014JE004626.

Liang, Q., Chen, C., Kaban, M.K., Thomas, M., 2019. Upper-mantle density structure in the Philippine Sea and adjacent region and its relation to tectonics. Geophys. J. Int. 219 (2), 945–957. https://doi.org/10.1093/gji/ggz335.

Luccio, F.Di., Pasyanos, M.E., 2007. Crustal and upper-mantle structure in the Eastern Mediterranean from the analysis of surface wave dispersion curves[J]. Geophys. J. Int. 1139–1152. https://doi.org/10.1111/j.1365-246X.2007.03332.x.

Mart, Y, Robertson, A H F, Woodside, J M, 1997. Cretaceous tectonic setting of Eratosthenes Seamount in the eastern Mediterranean Neotethys[J]. initial results of ODP Leg 160[J]. Comptes rendus de l'Académie des sciences. Série 2. Sciences de la terre et des planètes 324 (2), 127–134.

McBRIDE, 1990. Seismic inMcBride_Palmyrides_AAPG_90.

Meier, T., Dietrich, K., St, B., Harjes, H., Meier, T., 2004. One-dimensional models of shear wave velocity for the eastern Mediterranean obtained from the inversion of Rayleigh wave phase velocities and tectonic implications. MY PL IN 45–58. https://doi.org/10.1111/j.1365-246X.2004.02121.x.

Mooney, W.D., Kaban, M.K., 2010. The north American upper mantle: Density, composition, and evolution. J. Geophys. Res. Solid Earth 115 (12), 1–24. https://doi.org/10.1029/2010JB000866.

Netzeband, G.L., Gohl, K., Hübscher, C.P., Ben-avraham, Z., Dehghani, G.A., Gajewski, D., Liersch, P., 2006. The Levantine Basin — crustal structure and origin, 418, pp. 167–188. https://doi.org/10.1016/j.tecto.2006.01.001.

Ritsema, J., Deuss, A., Van Heijst, H.J., Woodhouse, J.H., 2011. S40RTS: a degree-40 shear-velocity model for the mantle from new Rayleigh wave dispersion, teleseismic traveltime and normal-mode splitting function measurements. Geophys. J. Int. 184 (3), 1223–1236. https://doi.org/10.1111/j.1365-246X.2010.04884.x.

Robertson, A.H.F., 1998. Formation and destruction of the Eratosthenes Seamount, eastern Mediterranean Sea, and implications for collisional processes. Proc. Ocean Dril. Prog. Scientific Results 160, 681–700. https://doi.org/10.2973/odp.proc.sr.160.063.1998.

Robertson Alastair, H.F., 1998. Tectonic significance of the Eratosthenes Seamount : a continental fragment in the process of collision with a subduction zone in the eastern Mediterranean (Ocean Drilling Program Leg 160). Tectonophysics 298, 63–82.

Robertson, A.H.F., Emeis, K.C., Richter, C., Blanc-Valleron, M.M., Bouloubassi, I., Brumsack, H.J., Woodside, J.M., 1998. Collision-related break-up of a carbonate platform (Eratosthenes Seamount) and mud volcanism on the Mediterranean Ridge: preliminary synthesis and implications of tectonic results of ODP Leg 160 in the Eastern Mediterranean Sea. Geol. Soc. Spec. Publ. 131, 243–271. https://doi.org/10.1144/GSL.SP.1998.131.01.16.

Root, B.C., Ebbing, J., van der Wal, W., England, R.W., Vermeersen, L.L.A., 2017. Comparing gravity-based to seismic-derived lithosphere densities: a case study of the British Isles and surrounding areas. Geophys. J. Int. 208 (3), 1796–1810. https://doi.org/10.1093/gji/ggw483.

Schaeffer, A.J., Lebedev, S., 2013. Global shear speed structure of the upper mantle and transition zone. Geophys. J. Int. 194 (1), 417–449. https://doi.org/10.1093/gji/ggt095.

Seber, D., Sandvol, E., Sandvol, C., Brindisi, C., Barazangi, M., 2001. Crustal model for the Middle East and North Africa region: Implications for the isostatic compensation mechanism. Geophys. J. Int. 147 (3), 630–638. https://doi.org/10.1046/j.0956-540x.2001.01572.x.

Segev, A., Rybakov, M., Lyakhovsky, V., Hofstetter, A., Tibor, G., Goldshmidt, V., Ben Avraham, Z., 2006. The structure, isostasy and gravity field of the Levant continental margin and the Southeast Mediterranean area. Tectonophysics 425 (1–4), 137–157. https://doi.org/10.1016/j.tecto.2006.07.010.

Simmons, N.A., Myers, S.C., Johannesson, G., Matzel, E., Grand, S.P., 2015. Evidence for long-lived subduction of an ancient tectonic plate beneath the southern Indian Ocean, pp. 9270–9278. https://doi.org/10.1002/2015GL066237.

Smit, J., Brun, J.P., Cloetingh, S., Ben-Avraham, Z., 2010. The rift-like structure and asymmetry of the Dead Sea Fault. Earth Planet. Sci. Lett. 290 (1–2), 74–82. https://doi.org/10.1016/j.epsl.2009.11.060.

Steinberger, B., Calderwood, A.R., 2006. Models of large-scale viscous flow in the Earth's mantle with constraints from mineral physics and surface observations. Geophys. J. Int. 167, 1461–1481.

Stern, R.J., Johnson, P., 2010. Continental lithosphere of the Arabian Plate: a geologic, petrologic, and geophysical synthesis. Earth Sci. Rev. 101 (1–2), 29–67. https://doi.org/10.1016/j.earscirev.2010.01.002.

Stixrude, L., Lithgow-Bertelloni, C., 2005. Thermodynamics of mantle minerals—I. Physical properties. Geophys. J. Int. 162, 610–632.

Stolk, W., Kaban, M., Beekman, F., Tesauro, M., Mooney, W.D., Cloetingh, S., 2013. High resolution regional crustal models from irregularly distributed data: Application to Asia and adjacent areas. Tectonophysics 602, 55–68. https://doi.org/10.1016/j.tecto.2013.01.022.

Tang, Z., Mai, P.M., Julià, J., Zahran, H., 2019. Shear velocity structure beneath saudi arabia from the joint inversion of P and S wave receiver functions, and rayleigh wave group velocity dispersion data. J. Geophys. Res. Solid Earth 124. https://doi.org/10.1029/2018JB017131.

Tesauro, M., Kaban, M.K., Mooney, W.D., Cloetingh, S.A.P.L., 2014. Density, temperature and composition of the north American lithosphere: New insights form a joint analysis of seismic, gravity and mineral physics data. Part II: thermal and compositional model of the upper mantle. Geochem. Geophys. Geosyst. 15, 4781–4807. https://doi.org/10.1002/2014GC005484.Welford.

Vannucchi, P., Sage, F., Phipps Morgan, J., Remitti, F., Collot, J.Y., 2012. Toward a dynamic concept of the subduction channel at ero- sive convergent margins with implications for interplate material transfer. Geochem. Geophys. Geosyst. 13, Q02003. https://doi.org/10.1029/2011GC003846.

Welford, J.K., Hall, J., Christian, H., Louden, K., 2015. Crustal seismic velocity structure from Eratosthenes Seamount to Hecataeus Rise across the Cyprus Arc, eastern Mediterranean[J]. GJI Geodyn. Tecton. 200, 935–953. https://doi.org/10.1093/gji/ggu447.

Wen, Z., Tong, X., Gao, H., Wang, Z., Chen, R., Song, C., Kang, H., 2021. Build-ups and hydrocarbon accumulation of the isolated carbonate platforms in the eastern Mediterranean. Pet. Explor. Dev. 48 (2), 323–336. https://doi.org/10.1016/S1876-3804(21)60026-5.

Makris, J., Papoulia, J., Wang, J., 2021. 3D sediments and crustal structure of the eastern Mediterranean basin derived from gravity data. *3rd EAGE Eastern Mediterranean Workshop*, (December 2021), pp. 10–12. https://doi.org/10.3997/2214-4609.202137016.

Kaban, M.K., Petrunin, A., Mooney, W., 2013. Cratonic roots under North America are shifted by basal drag: New evidence from gravity and geodynamic modeling[C]. Abstract T21C-05, Fall Meeting, AGU, San Francisco, Calif, 9–13 Dec.

Schattner, U., 2010. What triggered the early-to-mid Pleistocene tectonic transition across the entire eastern Mediterranean[J]. Earth Planet. Sci. Lett. 289, 539–548.

Khair, K., Tsokas, G.N., 1999. Nature of the Levantine (eastern Mediterranean) crust from multiple-source Werner deconvolution of Bouguer gravity anomalies. J. Geophys. Res. Solid Earth 104 (B11), 25469–25478. https://doi.org/10.1029/1999jb900228.

Eppelbaum, L., Katz, Y., 2015. Eastern Mediterranean: Combined geological–geophysical zonation and paleogeodynamics of the Mesozoic and Cenozoic structural-sedimentation stages[J]. Mar. Pet. Geol. 65, 198–216.